DOE award #: DE-SC-0010399
Recipient: West Virginia University Research Corporation
Project Title: Develop On-Demand nanoplasmonic Device Concepts in a Semiconductor Compatible Hybrid System
PI: Cheng Cen

This work was generated with financial support from the U.S. Government through Award No. DE-SC-0010399 and as such the U.S. Government retains a paid-up, nonexclusive, irrevocable, world-wide license to reproduce, prepare derivative works, distribute copies to the public, and display publicly, by or on behalf of the Government, this work in whole or in part, or otherwise use the work for Federal purposes.

Abstract

This report summarizes the research activities supported by the U.S. Department of Energy grant DE-SC-0010399. The goal of this project is to is to develop an on-demand nanoplasmonic platform that combines emerging oxide nanoelectronics with a low-loss semiconductor-friendly plasmonic materials. Toward this goal, several unique heterostructures formed between complex oxides and 2D layered materials have been developed. Based on these material systems, a set of atomic force microscope (AFM) based techniques have been developed that can allow long-living and reversible material phase transitions to be manipulated in nanoscale at room temperature. Using such technique and through interface coupling, we can effectively tune the plasmon propagations in unconventional plasmonic materials such as graphene and VO_2. In addition, we also discovered a plethora of novel interface enabled electro-optic effects, including the spatial modulation of light using 2DEG, a giant programmable photothermoelectric effects at room temperature, a light induced superconducting transition, and a tunable giant third order optical nonlinearities. These major results are outlined in this report, along with lists of project participants and products.

Significant Results

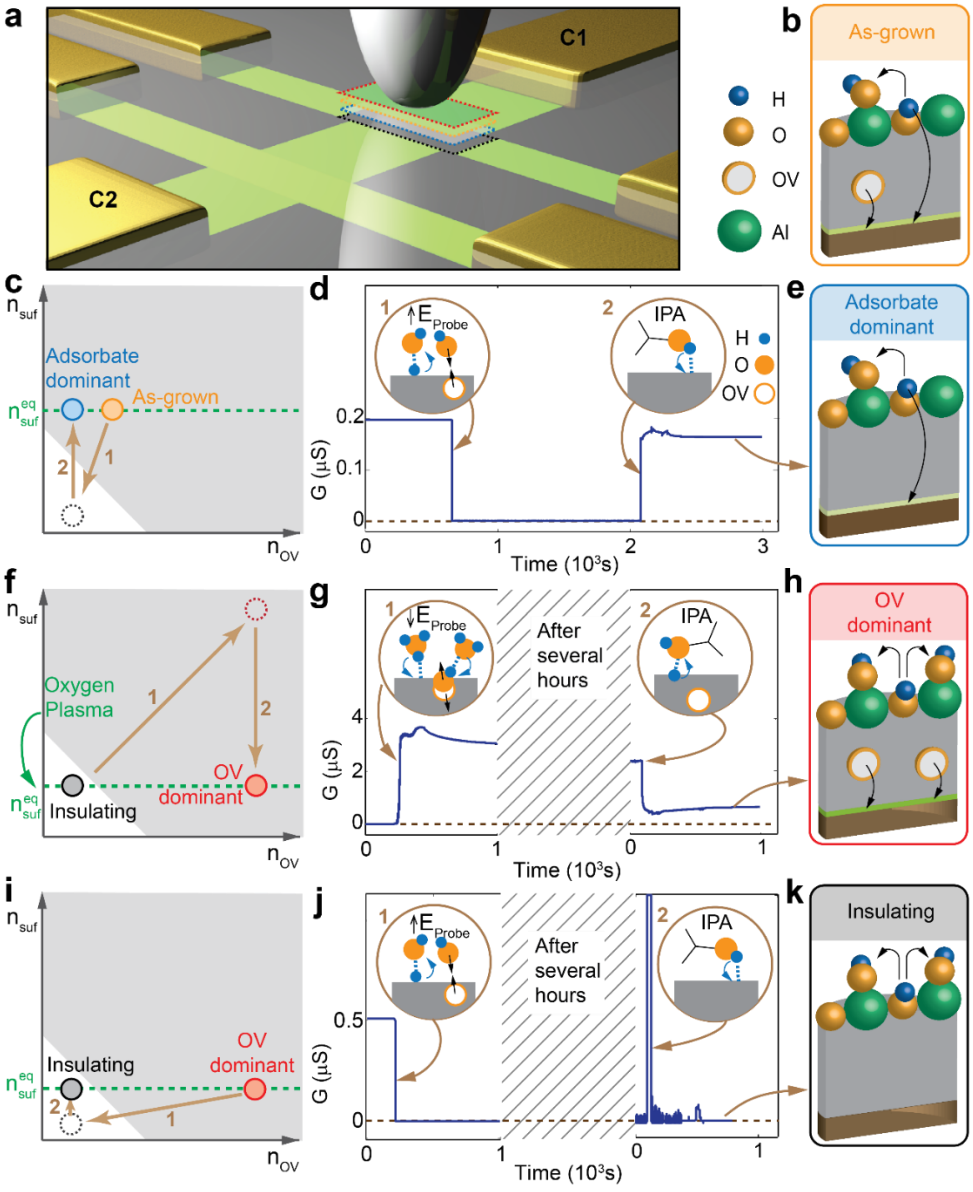

Figure 1 *Methodology used in controlling the interface doping mechanisms. (a) Interface region (enclosed by dashed lines) were reconfigurably patterned with 2DEG forming from distinct doping mechanisms (as illustrated in b,e,h,k). (c, f, i) Schematic diagrams showing the relative doping contributions from the surface adsorbates (nsurf) and oxygen vacancies (nov) in stable (solid circles) and metastable (dashed circles) interface states. When the transitions between different states were induced experimentally following the sequences as shown by brown arrows, interface conductance changes monitored between the interface contacts labeled as "C1" and "C2" are plotted in (d, g, j). Circular insets show the working principles of how each transition was controlled.*

At $LaAlO_3/SrTiO_3$ (LAO/STO) interfaces, the interplay between multiple doping mechanisms leads to the complexity of this system but also gives rise to a series of fascinating properties. To elucidate these entangled properties, it is important not only to have control over the metal-insulator transition by the net doping effects, but also to gain the capability of tuning individual doping mechanism in parallel. We have achieved this task in nano to microscopic scales by combining intensive local field generated by conducting atomic force microscope (c-AFM) probe which controls both the creation/migration of oxygen vacancies and the surface proton density, with plasma assisted surface hydroxylation and solvent based proton solvation that act mainly on surface adsorbates. Using this method, on-demand 2DEG nanostructures formed from tailored doping mechanisms can be created with a wide range of tunable carrier properties.

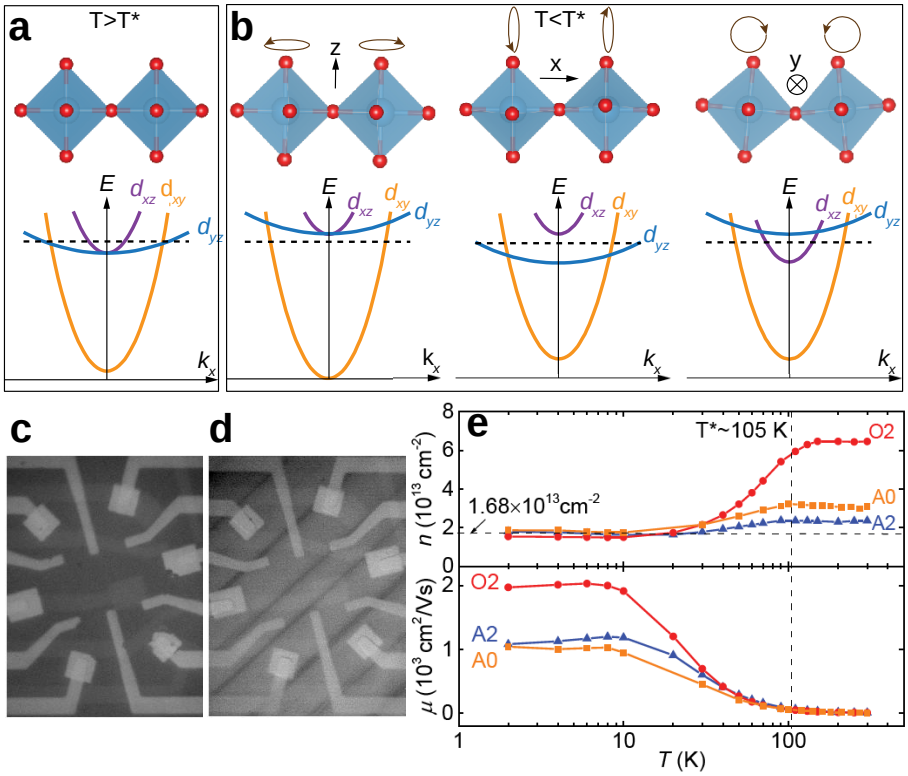

Figure 2 Tailor subband occupations in c-AFM created interface 2DEG structures *(a) Room temperature cubic structure of $SrTiO_3$ lattice and the light (d_{xy}) and heavy (d_{xz}, d_{yz}) subbands formed from interface 2DEG confinement. (b) In the low temperature tetragonal phase, AFD octahedral rotations in different orientations shift each subband differently and can lead to spatially varying subband occupations that are difficult to distinguish in macroscopic transport measurements. (c) Optical birefringence image of a device area on an out-of-plane z-domain. (d) Optical birefringence image of a second device area on interleaved domains in x and y orientations, where 45-degree domain walls can be clearly seen. (e) Temperature dependent carrier density and mobility of a conducting channel created inside z-domain device area by c-AFM. The tetragonal phase transition at around 105 K shift the two heavy bands above the Fermi level. This effect*

leads to a single band low temperature transport with a universal carrier density around $1.68\times10^{13}cm^{-2}$ *regardless of its room temperature values.*

A strong correlation between octahedral rotations in $SrTiO_3$ (STO) substrate and the interface 2DEG subband occupations was discovered. Below 105K, STO undergoes a structural phase transition from cubic to tetragonal phase with antiferrodistortive (AFD) oxygen octahedral rotations (Fig.2a, b). The broken inversion symmetry by such AFD rotations, together with the two dimensional confinement potential at the interface, lift the degeneracy of Ti t_{2g} orbitals (*xy, xz, yz*) and lead to drastically different transport properties in these different subbands. Using optical birefringence, we were able to accurately identify domains with different octahedral rotation axis and therefore different alignments of subbands (Fig.2c, d). By performing c-AFM writing in these identified domains, we successfully created conducting channels with tailored subband occupations that can be characterized by subsequent magnetotransport measurements (Fig.2e). The capability of understanding and engineering subband structures in oxide 2DEG is very important for the further heterostructure design.

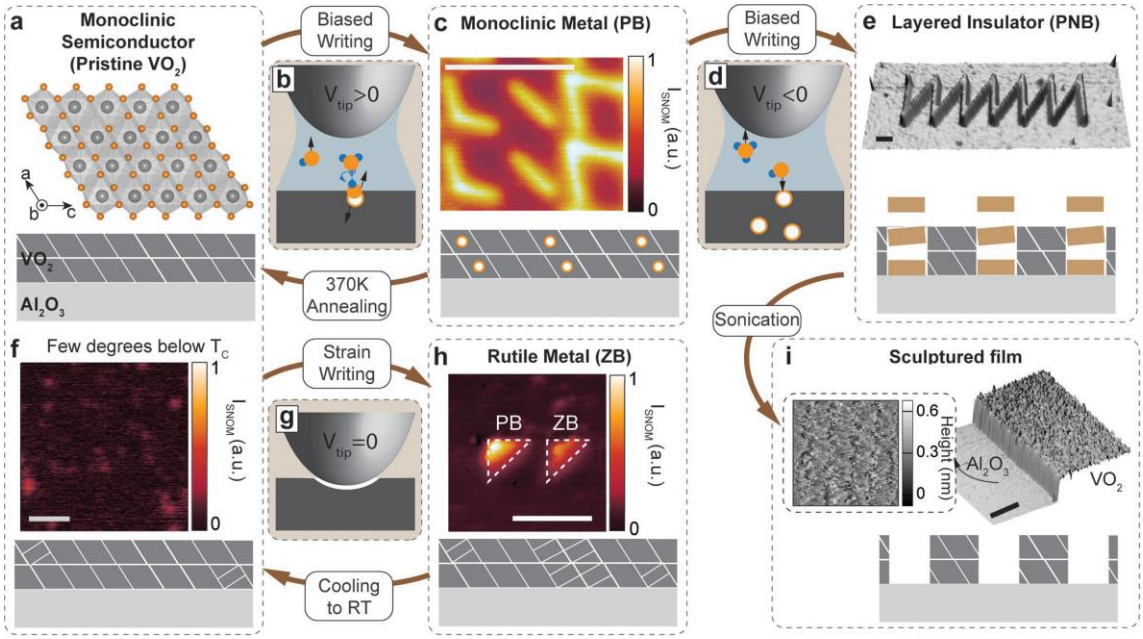

Figure 3. *AFM probe controlled phase transitions. a) Monoclinic semiconducting state of pristine VO2 film. b) Positive probe bias induced surface electrochemical process locally creates a monoclinic metallic phase (PB). c) Scanning near-field optical microscopy (SNOM) image shows a metasurface pattern of PB structures written by AFM. Annealing the sample above Tc erases the PB phase, restoring pristine* VO_2*. d) Subsequent negative probe bias (PNB) induced surface electrochemical process further transforms the PB*

phase into a van der Waals layered insulating compound. e) AFM image shows the 50% lattice expansion in PNB structures. i) This layered compound can be completely removed by sonication and leads to a nanosculptured film. AFM image shows the locally exposed Al_2O_3 terraces after the removal of PNB structure. f) By heating the pristine film to a few degrees below TC, onset of rutile phase occurs. g) At such temperatures, strain applied by AFM probe can switch the contact area into rutile phase (ZB). h) SNOM image shows a strain-induced ZB structure and a bias-induced PB structure side-by-side. ZB structure restores to pristine after beingcooled to RT. All scale bars indicate 1 μm.

While the tip controlled metal-insulator transition at $LaAlO_3/SrTiO_3$ interface is most significant in tuning the electrical properties, a similar process triggered in VO_2 thin films can produce drastic changes in the material's structural and optical characteristics. We succeeded in realizing reconfigurable nanoscale manipulations of VO_2 thin films from the pristine monoclinic semiconducting phase to either a stable monoclinic metallic phase, a metastable rutile metallic phase, or a layered insulating phase, all at room temperature, using an atomic force microscope (Fig.3).

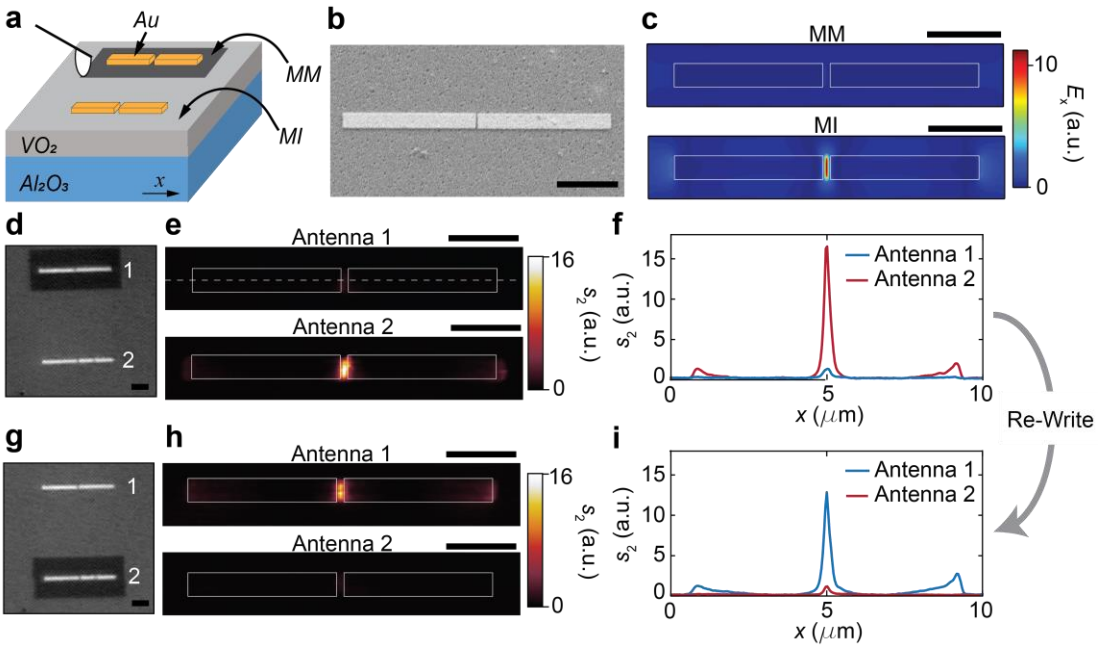

Figure 4 On-demand spatially modulated plasmonic resonances by AFM written VO_2 phases (a) *Illustration of a scanning probe locally inducing the MM phase around an Au gap-antenna.* ***(b)*** *Scanning electron microscope (SEM) image of the Au gap antenna fabricated on VO_2 film surface.* ***(c)*** *FDTD simulations of the in-plane field distributions at a detection plane 60 nm above the gold antennas surrounded by MM-phase (top) or MI-phase (bottom) VO_2.* ***(d)*** *Optical images of two same antennas next to each other. Antenna-1 is surrounded by AFM-written MM-phase VO_2, while the VO_2 film near antenna-2 is left in the as-grown MI phase.* ***(e)*** *Corresponding SNOM images of the two antennas.*

Local "hot spot" is only detected in antenna-2. ***(f)*** *SNOM line profiles along the two antennas.* ***(g-i)*** *Same as (d-f) but after an AFM-rewrite that erases the MM-phase rectangle surrounding antenna-1 and has another one patterned near antenna-2. Scale bars in this figure all represent 2 μm.*

Using this technique, rewritable mid-infrared plasmonic devices such as waveguides, spatially modulated plasmonic resonators (Fig.4), and reconfigurable wire-grid polarizers are successfully developed, demonstrating a promising monolithic nanoplasmonic platform for tailored optical functionalities at infrared frequencies.

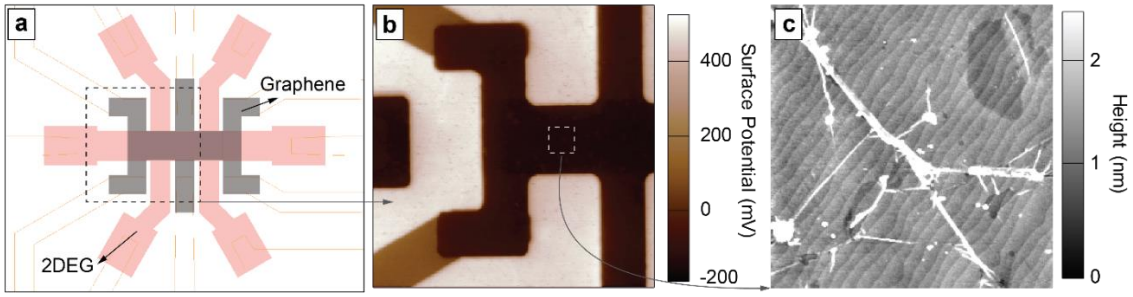

Figure 5 Double-layer hall bar structure fabricated from graphene on top of oxide 2DEG*. (a) Schematic showing the graphene hall bar positioned on top of 2DEG Hall bar at LAO/STO interface. (b) KPFM imaging on part of the structure. The region covered by Graphene has much lower surface potential. (c) Topography image showing graphene on top of LAO/STO. Wrinkles are from transferred CVD graphene, and monolayer terraces are from LAO/STO.*

High quality dual hall bar structures was fabricated (Fig.5) which not only allows the transport properties of graphene and oxide 2DEG in graphene/$LaAlO_3$(LAO)/$SrTiO_3$(STO) heterostructure to be separately studied, but also enables the investigations between the two layers separated only by several monolayers of LAO.

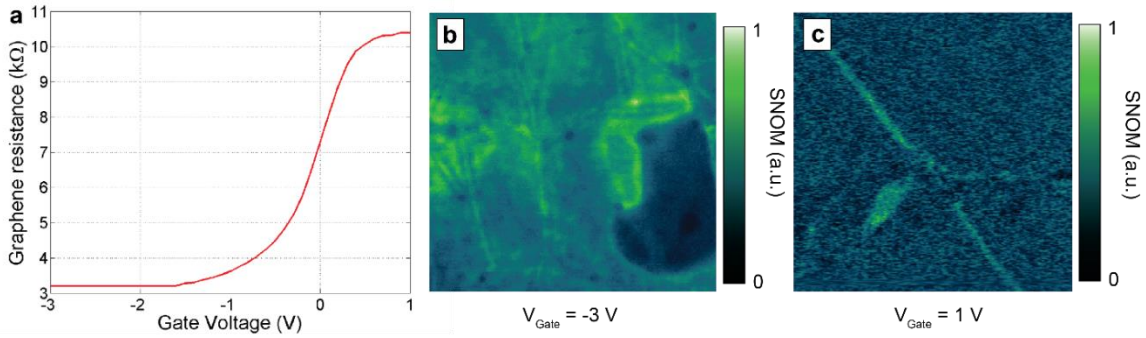

Figure 6 Tuning the electronic properties of graphene by biasing oxide 2DEG *(a) Graphene resistance change as a function of voltage applied to interfacial 2DEG. Dirac point in graphene was not reached due to the mutual gating effect, that is, interface 2DEG was depleted at large gate bias. (b) Away from Dirac point, SNOM images on graphene with a larger carrier density shows clear plasmon oscillations at grain boundaries. (c) Close to Dirac point, plasmon modes were suppressed due to the reduced carrier density.*

The electrical properties of graphene can be sensitively tuned by small biases applied to oxide 2DEG at LAO/STO interface. CVD graphene after transfer and patterning is p-type doped. Increasing the hole density by applying a negative bias to the interface 2DEG, clear 2D plasmon oscillations in graphene can be observed by scattering based near field scanning optical microscope (SNOM). When the hole density was suppressed, plasmon mode ceased to exist. We also identified a problem when using interface 2DEG in as-grown state to gate the graphene: we were unable to gate graphene to n-type regime by applying positive bias to the interface 2DEG. The resistance of graphene saturated before the Dirac point can be reached. This is because of the mutual coupling between graphene and n-type oxide 2DEG: while more electrons were being added to the graphene, carriers were also being depleted from the interface 2DEG. Once the conductance at LAO/STO interface was completely suppressed by such depletion process, it can no longer serve as a bottom gate for graphene.

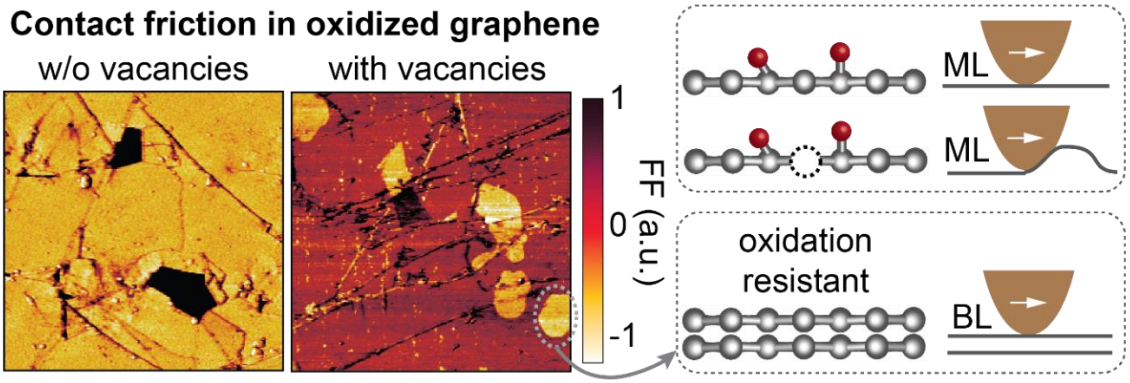

Figure 7 Frictional force image in graphene with oxygen add-atoms *(left) and graphene with vacancies (middle). In presence of vacancies, the contact friction of graphene became significantly larger, which can be understood by considering the reduced elastic stiffness and the resultant puckering at contact edge (right, top). Bilayer graphene exhibited great oxidation resistance, which remained in pristine state when monolayer graphene was already significantly modified.*

In the fabricated graphene/LAO/STO heterostructures, we found that, graphene on the complex oxide substrate is much easier to oxidize comparing to conventional SiO_2/Si

substrate. By controllably oxidizing graphene using shielded oxygen plasma and reducing it by short wavelength laser illumination graphene on oxide substrates, we were able to produce modified graphene with a large contact friction. This effect was attributed to the vacancies formed during the reduction process (Fig.7). Vacancies enhance the out-of-plane deformation flexibility in graphene, which tends to produce large puckering of graphene sheet near the contact edge and thus increases the effective contact area. Additionally, we also found that the bilayer graphene exhibits much larger oxidation resistance than monolayer graphene on complex oxides and therefore is a better choice in applications that requires good chemical stability.

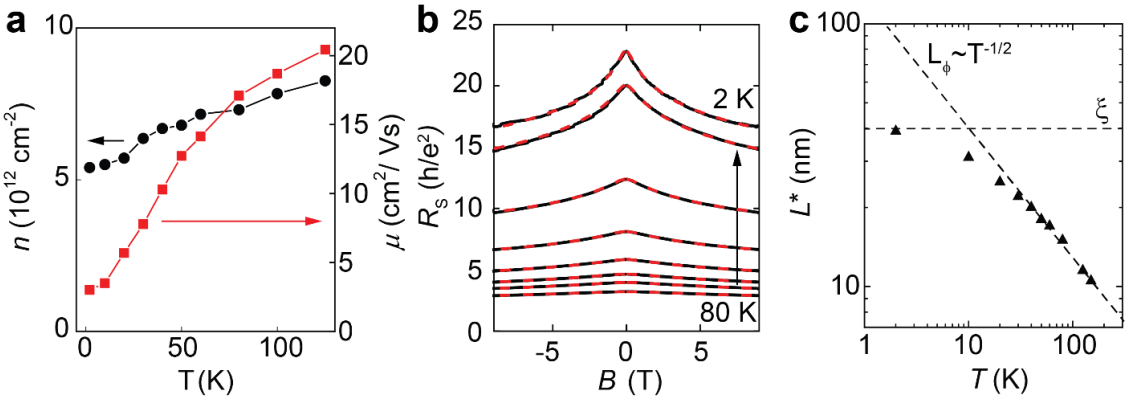

Figure 8 Localization effect at high defect density *(a) Temperature dependent carrier density and mobility measured in graphene at* τ_{OP} *= 138 s. (b) Magnetoresistance measured at various temperatures. Black solid lines are original data and red dash lines are fitting using weak localization model as described by Eq.1. (c) Temperature dependence of the characteristic length L* extracted from the fitting. At higher temperatures L* is dominated by the phase coherence length* $L_\phi \sim T^{-1/2}$*. As* L_ϕ *increases at low temperatures, L* becomes more significantly affected by the temperature independent localization length* ξ*.*

Modified graphene with large contact friction was heavily defected but remained a good electrical conductor. Such property is highly desirable in applications, such as triboelectric devices, which demands both large surface friction and conducting channels for charge harvest. These samples are also good platforms to study the unique transport behaviors in heavily disordered Dirac system, in which quantum interference effects at room temperature as well as the transition into strong localization regime were observed (Fig.8).

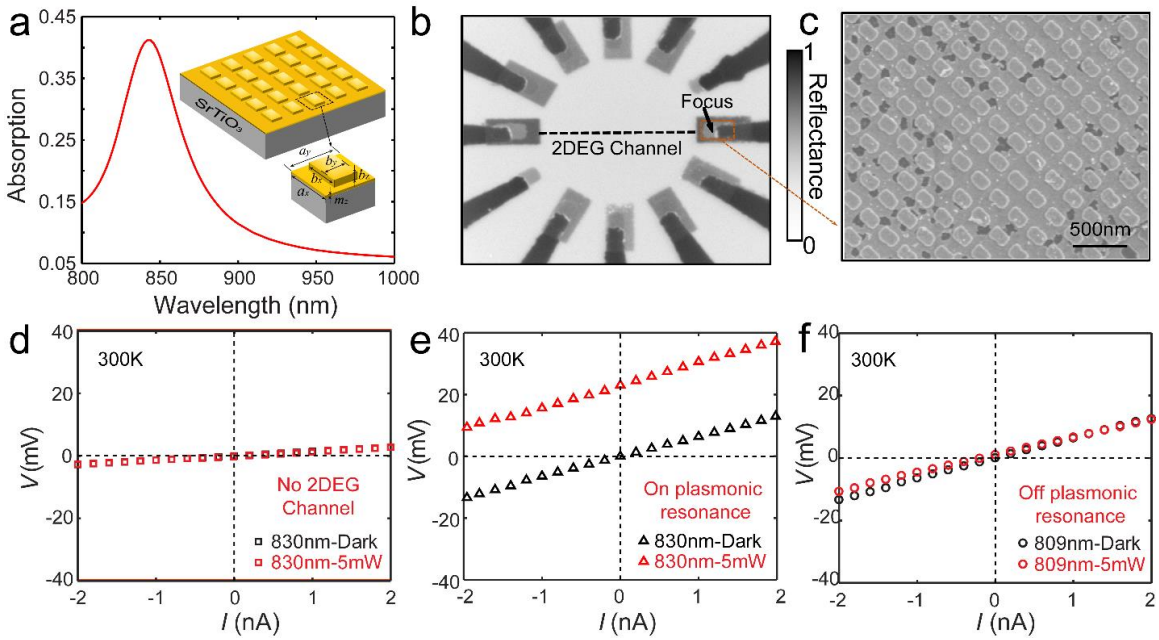

Figure 9 Large photothermoelectric (PTE) voltage generated by two-dimensional electron gas (2DEG) channels contacted with nanocubroid plasmonic light absorbers *(a) Numerical absorption spectrum of the nanocubroid array with shape parameters: a_x =250 nm, a_y =250 nm, b_x=180 nm, b_y=120 nm, b_z=30 nm, m_z=10 nm. (b) Optical image of the device area. (c) SEM image of the nanocubroid array. (d, e) I-V curves measured at room temperature when a near-resonance 830nm laser beam was focused on the patterned electrode in presence of 2DEG channel (e) and after the 2DEG channel is erased (d). (f) I-V curves when a off-resonance 809nm laser beam is focused on the patterned electrode connected by 2DEG channel*

To maximize the photovoltaic efficiency, it is highly desirable to enable the electricity conversion from low energy photons and to extract the excessive energy from hot carriers. We have successfully achieved a large photovoltage generation at the $LaAlO_3/SrTiO_3$ (LAO/STO) interfaces from infrared photons with energies far below the oxide bandgaps, utilizing the photoexcitations of hot carriers in metal contacts. By controlling the local interface metallicity near the contact region using conducting atomic force microscope (c-AFM), two different light-charge conversion mechanisms can be selected. The first of them, originating from the band alignment induced hole filtering effect, is prominent only at low temperatures when the interfacial electron mobility is large. The second one, which requires the presence of two-dimensional electron gas (2DEG), is produced from the photothermoelectric (PTE) effect and significant at room temperature. In order to improve the light absorptance, metasurface structures made from plasmonic nanocubroid arrays are integrated on top of plain metal contacts (Fig.9). Such integration allows the infrared-

responsivity to reach 4.4 V/W at room temperature, which is much greater comparing to other infrared PTE generations reported in bulk complex oxide and 2D materials.

While the light-absorption performances of the plasmonic nanocubroid array used are wavelength-sensitive, their geometry parameters can be easily modified to suit different incident frequencies. Integrating multiple nanocubroid arrays with different plasmonic resonances on a single sample, it is also possible to achieve broadband yet programmable spectral responses by utilizing the reconfigurable 2DEG thermoelectric channels to selectively couple hot electrons generated by different frequencies of light. Such combination of metasurface techniques with spatially programable generation and routing of photovoltage is bound to bring forward new and exciting opportunities in light sensing and electro-optical applications.

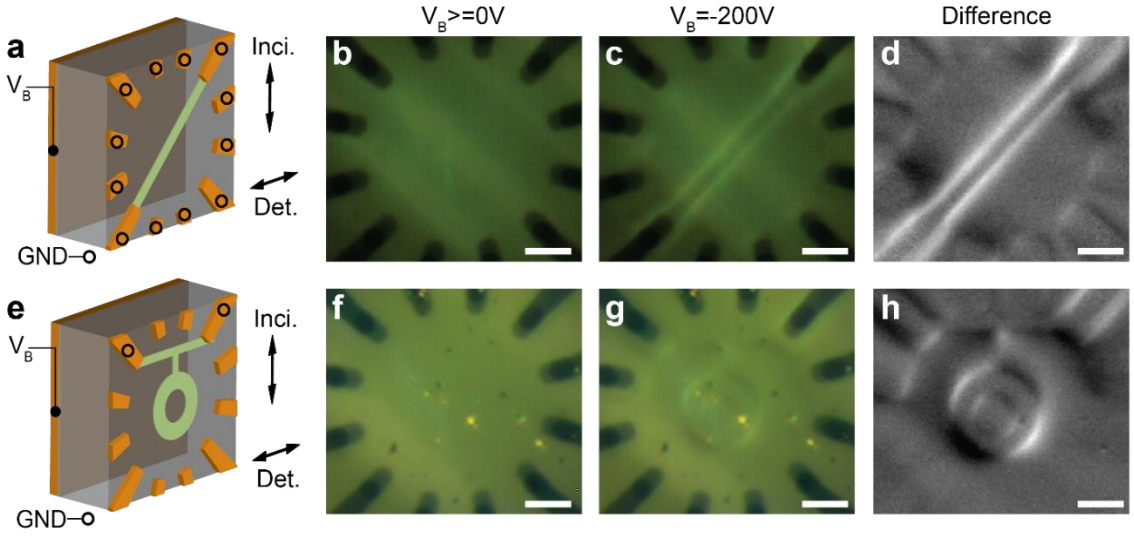

Figure 10 Electro-optic effect observed at the boundary of interface 2DEG structures *(a, e) Schematics showing the written 2DEG structures (green), electrode layouts (orange), and the biasing setups. (b, f) Polarized light microscope (PLM) images taken at 6 K under zero back bias. When positive back biases were applied, the obtained images showed no observable difference. (c, g) PLM images taken under -200 V back bias. (d, h) Difference images generated by subtracting the zero bias background from the negative bias images. Scale bars represent 10 μm.*

Gradient in the interfacial potential profile can be an useful tool for breaking the intrinsic structural symmetry in materials and generate new functionalities unavailable in macroscopic materials. For example, low density electronic systems, such as graphene and the 2DEG at oxide interface, usually cannot be detected by visible light. Their invisibility posed significant challenge in device fabrications. While the direct interactions

between low-density electronic systems and visible light are weak, it might be more effective to generate indirect coupling through other degrees of freedom in the material. We found that, 2DEG structures formed at complex oxide interfaces, which are optically transparent on their own, can be conveniently imaged using visible light microscope by producing field-induced polar transition in the lattice (Figure 10). Besides of enabling direct visualization, optical imaging also provided a unique opportunity to monitor how spatially confined electronic systems respond to field-effect, especially in the low carrier density regime where electrical measurements become challenging. The measurement results identified the polar axes associated with the field-induced symmetry breaking, and also allowed us to capture a shock-wave alike slow electron depletion process driven by field-emission. In addition, by varying the interface 2DEG patterns, different rewritable spatial light modulation configurations can be flexibly generated, manifesting new possibilities in on demand nanophotonic applications.

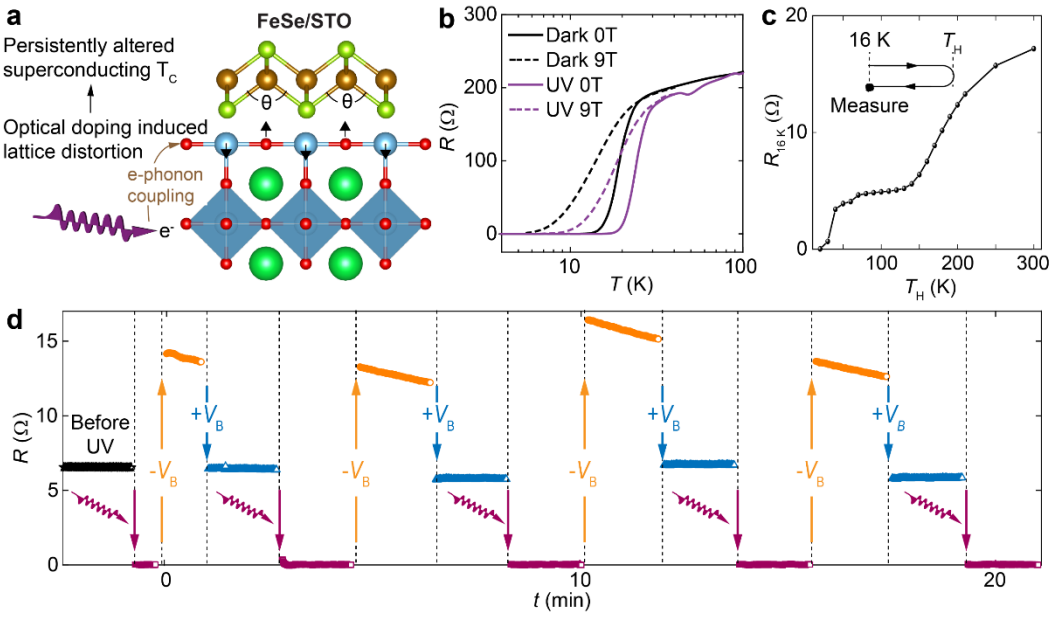

Figure 11 Light induced non-volatile switching of superconductivity in 1uc-FeSe/STO (a) UV excitation can cause persistent phonon softening $SrTiO_3$ and polar structural distortion at the interface. These effects can be utilized to control the superconducting state in FeSe grown on top. (b) Temperature dependent resistances measured in 1uc-FeSe/STO (capped by 10 uc FeTe) with and without UV illumination or external magnetic field. (c) A series of thermal cycles of 16 K → T_H → 16 K were performed after turning off the UV light. At the end of each thermal cycle, sample resistance at 16 K was measured and plotted as a function of the maximum temperature (T_H) reached during sample heating.(d) Non-volatile switching between normal and superconducting states at 17 K by sequence of UV light pulses and back bias voltage pulses.

The strong electron-phonon correlations in 3D complex oxides can be used to manipulate the superconductivity pairing in 2D vdW films through interface coupling (Fig.11). We have successfully demonstrated the optical gating in 1uc-FeSe/STO (capped by protective FeTe layers). A brief exposure to a weak (~10^1 μW /cm^2) continuous wave (CW) ultraviolet (UV) light, with photon energy above the optical bandgap of STO, can raise the superconducting TC in 1uc-FeSe/STO by 25% and generate a zero-resistance state persistent in dark for at least days. The full recovery to the normal state requires thermal cycling to room temperature, with the most significant change occurring at the well-known phase transition temperatures of STO. Using tailored sequence of UV light pulses and voltage pulses applied to the back of the STO substrate, the heterostructure can be persistently driven between the metastable superconducting state and its normal ground state. We attribute this effect to the strong photocarrier-phonon coupling in STO and the resultant metastable polar lattice distortion occurred at the FeSe/STO interface. STO undergoes a quantum paraelectric phase transition at low temperatures, where quantum fluctuations associated with zero-point energy prevent the onset of long range ferroelectric order. In this phase, photoexcited electrons can quadratically couple to the T1u soft mode (relative displacement between the Ti ion and the oxygen octahedra). In particular, the polarons formed from photocarriers and phonons can serve as effective charge trap to suppress electron-hole recombination and generate local dipole moments. In FeSe/STO heterostructure, the interface band bending gives rise to a large electric field at the interface which points from STO to FeSe. In the presence of this field, the alignment of induced dipole moments at the interface may effectively modify the ferroelectric distortions with relative out-of-plane shifts between the Ti and O ions. As a result, it is viable that the Se-Fe-Se angle in the FeSe monolayer, a parameter sensitively modulating the electron correlation strength in FeSe, will be perturbed and lead to an enhanced T_C.

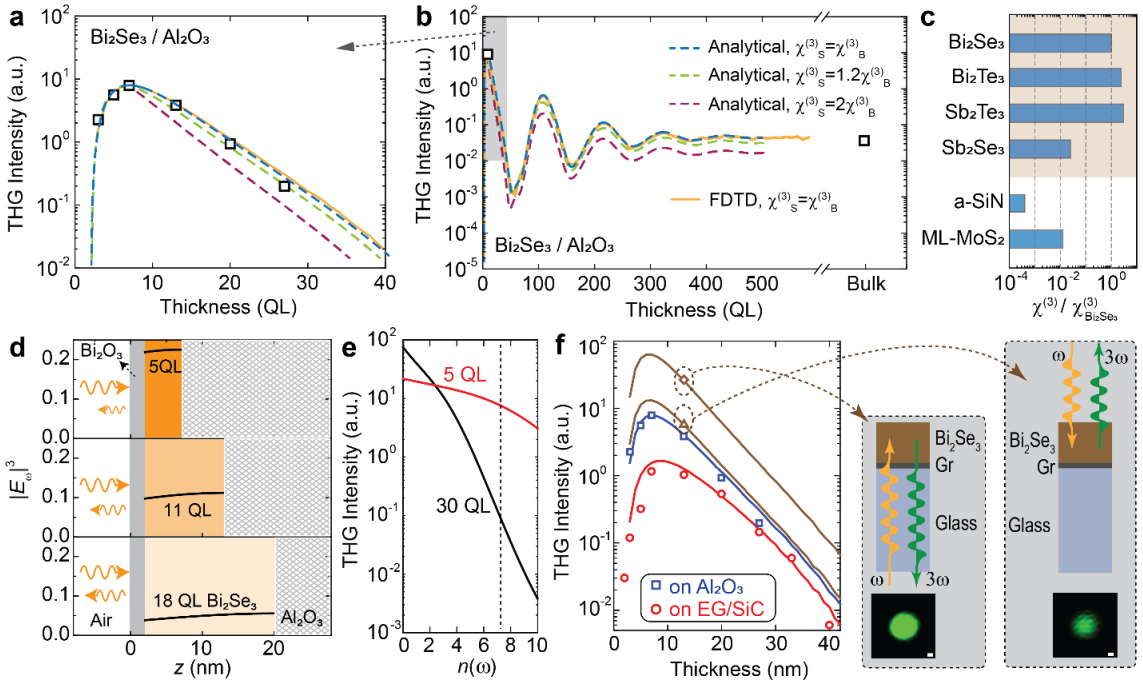

Figure 12 Substrate modulated giant nonlinear optical generations in topological insulator films *(a, b) FDTD and analytical models of the thickness dependent THG intensity considering three different $\chi^{(3)}$ spatial distributions: a constant $\chi^{(3)}$ throughout the film (blue dashed lines, orange solid lines); $\chi^{(3)}$ in the surface and interface layers is 1.2 times larger than the bulk value (green dashed lines), and $\chi^{(3)}$ in the surface and interface layers is 2 times larger than the bulk (purple dashed lines). Experimental data are plotted in black square dots. (c) Relative $\chi^{(3)}$ (normalized by the Bi_2Se_3 value) of different materials obtained by processing the experimental data using FDTD method. (d) Fundamental light field distribution inside Bi_2Se_3 for three different film thicknesses. (e) The calculated THG intensities in 5 QL and 30 QL films as functions of the real refractive index at the fundamental frequency ($n(\omega)$). The actual value of $n(\omega)$ is marked by the black dashed line. (f) Experimental data (scattered dots) and FDTD results (solid lines) comparing the THG intensities obtained in Bi_2Se_3 films grown on different substrates (Al_2O_3, EG/SiC, transferred graphene/glass slide). For the same 13 QL film grown on graphene/glass slide substrate, measurements performed with the fundamental light incident from the film side and the substrate side yields drastically different THG intensities. The inset microscopy images compare the reflected THG emission patterns measured using the two incidence geometries. Scale bars indicate 1 μm.*

We have discovered giant THG emissions in epitaxial V-VI chalcogenide TI films grown on different 3D bulk material substrates. The large 10^{-17}-10^{-16} m^2/V^2 level $\chi^{(3)}$ is found to be the product of the same bulk states that are involved in band inversion, and strongly benefit from the same material characteristics that enables the nontrivial topological ordering. We have also shown that, due to the highly nonlinear nature of these

processes, small variations in the heterostructure parameters can introduce drastic changes in the nonlinear output. Therefore, the correct interpretation of nonlinear performances in thin films requires systematic modeling and measurements within a large parameter space. The same feature also affords the tunability to further enhance the THG output by substrate/capping layer engineering. While several QLs of V-VI TIs can already rival microns of traditional NLO materials, due to the optical losses their NLO efficiency will not benefit from much longer optical paths. However, layered TIs have the unique advantage that their thin films can be readily grown by van der Waals epitaxy or mechanically transferred onto almost any substrates without precise lattice matching, allowing them to be integrated with many existing photonic or plasmonic architectures that can produce strong field enhancement in the near field. Such integrations can provide a viable alternative venue for NLO enhancement and produce nanoscale devices that are key to on-chip applications.

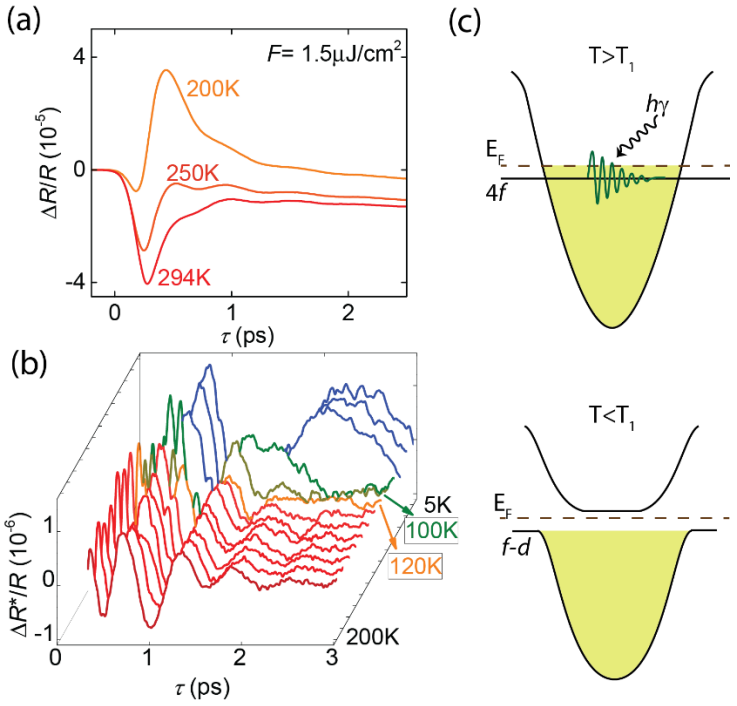

Figure 13: *Temperature dependence of f-band plasmon mode in SmB_6 (a) Pump induced reflectivity measurement of single crystal at high temperatures, showing a 1.7 THz oscillation signal. (b) Background subtraction is performed to emphasize the temperature dependence of the oscillating features. (c) Illustration of evolvement of plasmon at hybridization gap opening.*

Time resolved study of plasmon oscillations can provide valuable information on the plasmon damping mechanisms. The femtosecond resolution of optical pump-probe

experiments is particularly suitable for studying the terahertz plasmons supported by semiconducting systems (such as graphene and complex oxides). One example of our work in this area is shown in Figure 13, where characteristic heavy fermion plasmon oscillations were clearly observed. The temperature dependent evolvement of this mode reveals the band gap opening due to strong electron correlation effects.

Impact

The research conducted under this project successfully addressed several major challenges that the field of plasmonics is facing: 1. Low loss plasmonic materials allowing convenient interface to semiconductor electronics. 2. Deterministic guiding of long range plasmon mode with nanometer transverse confinement; 3. Information encoding in confined plasmon mode. Utilizing reconfigurable nanolithography techniques and completely semiconductor-friendly material stacks, the interface enabled tunable nanoplasmonic and electro-optic device concepts demonstrated in these works pave the way toward building future integrated nanophotonic circuits. Combining the abundant correlated properties in oxides with novel 2D materials, the heterostructures developed in this project also enables the investigation of interactions between plasmon mode and other material quanta such as phonon, spin and Cooper pairs, producing valuable fundamental knowledge in active quantum phase control.

Key Contributors

PI: Cheng Cen

Postdoc: Weitao Dai; Yi Liang; Yinxiao Xiang

Graduate Students: Sanjay Adhikari, Prakash Gajurel, Dustin Schrecongost

Unfunded Collaborators: Chang-Beom Eom (University of Wisconsin, Madison), Roman Engel Herbert (Pennsylvania State University), Haidan Wen (Argonne National Lab), Yoosuf N. Picard (Carnegie Mellon University), Jun Chen (University of Pittsburgh), Haitao Liu (University of Pittsburgh), Lian Li (West Virginia University), Yanjun Ma (Kurt J. Lesker)

Products

Journal Articles

- Yinxiao Xiang, Chenhui Yan, Fan Shi, Prakash Gajurel, Lian Li, Cheng Cen, "*Giant third-harmonic optical generation from topological insulator interfaces*", Nano Letters 21, 8872 (2021)

- Dustin Schrecongost, Yinxiao Xiang, Jun Chen, Cuifeng Ying, Hai-Tian Zhang, Ming Yang, Prakash Gajurel, Weitao Dai, Roman Engel-Herbert, and Cheng Cen, "*Rewritable Nanoplasmonics through Room-Temperature Phase Manipulations of Vanadium Dioxide*", Nano Letters 20, 7760 (2020)

- Weitao Dai, Yi Liang, Ming Yang, Dustin Schrecongost, Prakash Gajurel, Hyungwoo Lee, Jung-Woo Lee, Jun Chen, Chang-Beom Eom, Cheng Cen, "*Large and Reconfigurable Infrared Photothermoelectric Effect at Oxide Interfaces*", Nano Letters 19, 7149-7154 (2019)

- Dustin Schrecongost, Mina Aziziha, Hai-Tian Zhang, I-Cheng Tung, Joseph Tessmer, Ming Yang, Weitao Dai, Qiang Wang, Roman Engel-Herbert, Haidan Wen, Yoosuf N. Picard, Cheng Cen, "*On-demand nanoscale manipulations of vanadium oxide phases*", Advanced Functional Materials, 29, 1905585 (2019)

- Ming Yang, Chenhui Yan, Yanjun Ma, Lian Li, Cheng Cen, "*Light induced nonvolatile switching of superconductivity in single layer FeSe on $SrTiO_3$ substrate*", Nature Communications, 10, 85 (2019)

- Prakash Gajurel, Mina Kim, Qiang Wang, Weitao Dai, Haitao Liu, Cheng Cen, "*Vacancy Controlled Contact Friction in Graphene*", Advanced Functional Materials, 27, 1702832 (2017)

- Weitao Dai, Ming Yang, Hyungwoo Lee, Jung-Woo Lee, Chang-Beom Eom, and Cheng Cen, "*Tailoring the Doping Mechanisms at Oxide Interfaces in Nanoscale*", Nano Letters 17, 5620 (2017)

- Cen, Cheng, Yanjun Ma, Qiang Wang, and Chang-Beom Eom. "*Surface magnetism and proximity effects in hexaboride thin films*." Applied Physics Letters 110, 102404 (2017)

- Weitao Dai, Sanjay Adhikari, Andrés Camilo Garcia-Castro, Aldo H. Romero, Hyungwoo Lee, Jung-Woo Lee, Sangwoo Ryu, Chang-Beom Eom and Cheng Cen *"Tailoring $LaAlO_3/SrTiO_3$ Interface Metallicity by Oxygen Surface Adsorbates*" Nano Letters 16, 2739-2743, (2016)

- Sanjay Adhikari, Andrés C. Garcia-Castro, Aldo H. Romero, Hyungwoo Lee, Jung-Woo Lee, Sangwoo Ryu, Chang-Beom Eom, and Cheng Cen, "*Charge Transfer to $LaAlO_3/SrTiO_3$ Interfaces Controlled by Surface Water Adsorption and Proton Hopping*" Advanced Functional Materials 26, 5453-5459, (2016)

Submitted Manuscript

- Dustin Schrecongost, Hai-Tian Zhang, Roman Engel Herbert, Cheng Cen*, Oxygen Vacancy Dynamics of Monoclinic Metallic Vanadium Dioxide.* Submitted to Applied Physics Letters*.*

- Logan Lang, Hai-Tian Zhang, Prakash Gajurel, Ming Yang, Roman Engel Herbert, Cheng Cen, *Non-volatile, rewritable, all-optical imprinting in VO_2.* Submitted to Physical Review Applied.

- Ming Yang, Weitao Dai, Hyungwoo Lee, Jung-Woo Lee, Chang Beom Eom, Cheng Cen, *Programming spatial light modulations using mobile electrons.* Submitted to Science Advances.

- Yinxiao Xiang, Chenglin Du, Wei Wu, Cuifeng Ying, Mengxin Ren, Wei Cai, Jingjun Xu, Cheng Cen*l Taper-less nanoscale electromagnetic field concentration using plasmonic Tamm states.* Submitted to Optica

- Sanjay Adhikari, Yanjun Ma, Chang-Beom Eom, Cheng Cen, *Optical helicity control of surface current in SmB_6. Submitted to Physical Review B*

- Sanjay Adhikari, Yanjun Ma, Zach Fisk, Jing Xia, Chang-Beom Eom, Cheng Cen, *Ultrafast observation of electron hybridization and in-gap surface states formation in Kondo insulator SmB_6, Submitted to Physical Review B*

Conference presentations

- Weitao Dai, *Controlling the dual mechanisms of oxide interface doping*. 2017 APS March Meeting

- Yinxiao Xiang, *Topological insulator materials for advanced nonlinear in-chip plasmonic devices*. 2019 APS March Meeting

- Dustin Schrecongost *Nanophotonic Engineering of Reconfigurable Vanadium Dioxide Phases*. 2020 APS March Meeting

- Cheng Cen, *Giant Third-Harmonic Optical Generation from Topological Insulator Interfaces*. 2019 MRS Fall

- Logan Lang, *Metal-insulator transition based non-volatile, rewritable, all-optical imprinting on VO2*. 2018 APS March Meeting.

- Yinxiao Xiang, *High-efficient harmonic generation via Plasmonic Tamm states*. 2020 APS March Meeting.

- Ming Yang, *Light induced non-volatile switching of superconductivity in single layer FeSe/$SrTiO_3$*. 2018 APS March Meeting.

- Prakash Gajurel, *Vacancy Controlled Contact Friction in Graphene*. 2018 APS March Meeting.

- Cheng Cen, *Light Induced Non-Volatile Switching of Superconductivity in Single Layer FeSe on /$SrTiO_3$ Heterostructuressubstrate*. 2019 MRS Fall.

- Weitao Dai, *Metal-insulator transition at lanthanum aluminate-strontium titanate interface induced by oxygen plasma treatment*. 2016 APS March Meeting.

- Sanjay Adhikari, *Optical helicity control of surface current in SmB_6*. 2016 APS March Meeting.

- Pedram Tavadze, *Manipulating thin film properties by search for substrates over databases*. 2019 APS March meeting.

- Dustin Schrecongost, *Manipulating hot-electron based photovoltage generations at oxide interfaces*. 2018 APS March Meeting.

- Yanjun Ma, *Observation of Compensation Temperature in Epitaxial $Tm_3Fe_5O_{12}$ Thin Films by Polar Magneto-Optic Kerr Effect*. 2019 APS March Meeting.

- Ming Yang, *Optical properties of structurally modified VO_2*. 2016 APS March Meeting.

- Yanjun Ma, *Surface Magnetism and Proximity Effects in Hexaboride Thin Films*. 2018 APS March Meeting.

- Ming Yang, *Programming spatial light modulations using mobile electrons*. 2018 APS March Meeting.

Appendix

All published and submitted article files attached